Electron dynamics in unoccupied states of spatially aligned 7-a graphene nanoribbons on Au(788)

N. F. Kleimeier,[1,*] A. Timmer,[1] L. Bignardi,[1] H. Mönig,[1] X. L. Feng,[2] K. Müllen,[2] L. F. Chi,[1,3] H. Fuchs,[1,4] and H. Zacharias[1]

[1]*Physikalisches Institut, Westfälische Wilhelms-Universität, Wilhelm-Klemm Strasse 10, and Center for Nanotechnology, Heisenbergweg 11, 48149 Münster, Germany*

[2]*Max-Planck-Institute for Polymer Research, Ackermannweg 10, 55128 Mainz, Germany*

[3]*Institute of Functional Nano and Soft Materials (FUNSOM) & Collaborative Innovation Center of Suzhou Science and Technology, Soochow University, Suzhou, Jiangsu 215123, People's Republic of China*

[4]*Institute for Nanotechnology, Karlsruhe Institute of Technology, 76344 Karlsruhe, Germany*

(Received 3 September 2014; revised manuscript received 10 November 2014; published 3 December 2014)

Bottom-up synthesized armchair graphene nanoribbons with a width of seven C = C bonds (7-aGNRs) have gained widespread interest due to their large band gap of about 2.8 eV and their atomically precise edge structures. Here, we report on the lifetime of excited states of spatially aligned 7-aGNRs grown on a vicinal Au(788) surface. Time-resolved three-photon photoemission spectroscopy at $h\nu = 3.15$ eV was carried out to measure the lifetimes of states located at $E_1 - E_F = 3.6$ eV and $E_2 - E_F = 3.8$ eV via a resonant excitation from an unoccupied state at $E - E_F = 0.6$ eV. Lifetimes of $\tau_1 = (110 \pm 13)$ fs and $\tau_2 = (75 \pm 10)$ fs are observed, respectively.

DOI: 10.1103/PhysRevB.90.245408 PACS number(s): 78.47.D−, 62.23.Hj, 79.60.Jv

I. INTRODUCTION

Since its discovery by Novoselov *et al.* [1] graphene has stimulated intense research due to its remarkable electronic and mechanical properties. Since graphene is atomically thin, graphene-based transistors could be built smaller than conventional, silicon-based transistors, because short-channel effects are expected to be strongly suppressed when going to thinner gate layers [2]. Another highly desirable property for the application in transistors is the behavior of charge carriers as massless Dirac fermions, increasing the possible switching rates by several orders of magnitude [3]. Graphene, however, does not exhibit a band gap and therefore it is not suitable for many of these applications, resulting in graphene transistors with a very poor on/off ratio which will constantly consume power.

A promising route to achieve the opening of a band gap in graphene is the lateral confinement of the electrons in one direction. This can be obtained by cutting graphene sheets [4] or unzipping carbon nanotubes [5,6]. However, these approaches limit the width of the resulting nanoribbons to several nanometers, too large to open a significant band gap. Additionally, nanoribbons obtained with these methods have rough, undefined edges, which play an important role at this structure size. It has even been argued that in these nanoribbons the band gap is only a transport gap instead of a true gap between states from the conduction and valence bands [7]. To overcome these limitations, a bottom-up approach has been realized by Cai *et al.* [8], making it possible to grow atomically precise nanoribbons with a width of a few atoms and well-defined edges. By altering the width of the nanoribbons or by functionalization of their edges, the band gap can be tuned in the range of several eV [9,10]. Recently, it has been shown that it is possible to transfer these nanoribbons grown on gold onto insulating substrates and build FETs with saturation behavior [11].

To gain insight into the band structure of these nanoribbons, they can be grown on stepped high-index single crystals, as for example Au(788), forcing them to align along the length of the terraces of the crystal [12]. So far, experiments have have been focused on the band structure of the states close to the Fermi level by ultraviolet photoemission spectroscopy and inverse photoemission spectroscopy [12], two-photon photoemission [13], and scanning tunneling spectroscopy [14]. Here, we report on the relaxation dynamics of two excited states by time-resolved three-photon photoemission spectroscopy.

II. RESULTS AND DISCUSSION

Aligned 7-armchair graphene nanoribbons with a band gap of 2.8 eV were prepared under ultrahigh vacuum (UHV) conditions on a Au(788) crystal by subliming 10,10'-dibromo-9,9'-bianthryl (DBBA) as described previously [12]. Subsequently, the sample was transferred to the photoemission UHV chamber with a base pressure of 10^{-10} mbar. The chamber is equipped with a manipulator to heat the sample and to rotate it in front of the photoelectron detector which is composed of a time-of-flight tube and a multianode detector to record different $k_{||}$ simultaneously with an angular resolution of $\pm 2.5^\circ$. Before each measurement, the sample is heated up to 200 °C to clean it from possible contaminants. All experiments described in this paper were performed at room temperature with the graphene nanoribbons aligned horizontally along the rotation axis of the manipulator. A Ti:sapphire amplifier system delivering laser pulses at $\lambda_0 = 793$ nm with a pulse duration of $\tau = 35$ fs at a repitition rate of 6 kHz is used to pump an optical parametric amplifier for static one-color two-photon photoemission spectroscopy at different photon energies with pulse durations of $\tau = 120$ fs. With frequency doubled Ti:sapphire laser pulses time-resolved three-photon photoemission at $h\nu = 3.15$ eV with a pulse duration of $\tau = 28$ fs was carried out.

Figure 1 shows a photoelectron spectrum recorded at an excitation wavelength of $\lambda_0 = 285$ nm ($h\nu = 4.35$ eV). A fit to the spectral feature yields two overlapping states at kinetic energies of $E_{1,\mathrm{kin}} = (3.1 \pm 0.1)$ eV and $E_{2,\mathrm{kin}} = (3.4 \pm 0.1)$ eV. A linear offset (dotted line) and the cutoff by the Fermi edge (dashed line) were taken into account

*kleimeier@wwu.de

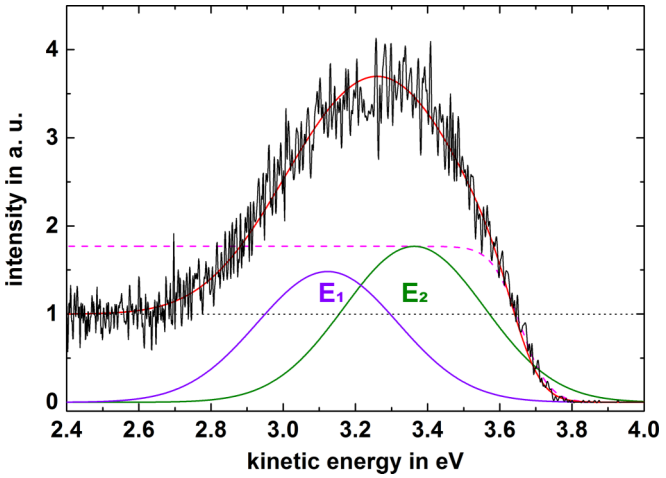

FIG. 1. (Color online) Two-photon photoemission spectrum of the 7-a GNRs excited with a photon energy of $h\nu = 4.35$ eV. The dotted line represents the linear background, the dashed line is the Fermi function convoluted with the response function of the detector and the two solid lines show the best fit to the two states we observed.

for the fit. To determine whether these states are occupied or unoccupied, we tuned the photon energy from $h\nu = 4.35$ to 3.94 eV in steps of about 0.07 eV (5 nm). Two-photon photoemission from an occupied state will then result in a change of the electron kinetic energy that is twice the change in photon energy, as the energy change of both photons has an influence. However, if the state is unoccupied, the binding energy of this state is fixed regardless of the photon energy for the first excitation step. Therefore only the energy change of the second excitation influences the kinetic energy: $\Delta E = \Delta h\nu$. The resulting spectra for different photon energies are shown in Fig. 2. All spectra are normalized to the linear part of the bulk emission background. It is evident that the spectral feature becomes narrower at lower photon energies, which is in line with the expectation for an unoccupied state. At lower photon energies, the higher-energy part of the state at E_2 cannot be populated anymore because its energetic distance from the Fermi edge is higher than the photon energy used for the excitation. Such assumption is confirmed by fitting a linear regression to the peak positions of the higher-lying state at E_2 (gray line in Fig. 2), which shows a slope of $m = (1.04 \pm 0.05)$. This confirms that only a single photon is required to emit a photoelectron from this state. Taking into account the work function of the sample which was determined to be 4.8 eV, it is possible to assign binding energies to both states. The states are thus located at $E_1 - E_F = (3.6 \pm 0.1)$ eV and $E_2 - E_F = (3.8 \pm 0.1)$ eV, respectively.

To determine the relaxation dynamics of the two unoccupied states, a better temporal resolution is required. This is achieved by frequency doubling the output of the Ti:sapphire amplifier to $h\nu = 3.15$ eV and recompressing the pulse in a prism compressor. Given the work function of the sample of $\phi = 4.8$ eV, a three photon process is required for resonant photoemission: two photons to populate the states at $E_1 - E_F = 3.6$ eV and $E_2 - E_F = 3.8$ eV and a third photon to emit the electrons from these states. At this wavelength the excitation is enhanced by a resonance between a state located at $E - E_F = 0.6$ eV as observed in the IPE measurement [12] and the final excited states. For time-resolved measurements, the pulses at 400 nm are split into two replicas in a Mach-Zehnder type interferometer. A dc motor driven delay stage (M- 405.DG, Physik Instrumente) allows to delay the pulses by $\Delta t = \pm 167$ ps with a resolution of 1 fs. A half-wave plate is inserted into the delay arm of the interferometer to rotate the plane of polarization of one of the replicas by 90° to avoid interference effects. The pulse duration at the position of the sample is measured by self-diffraction autocorrelation measurements in a BBO crystal with all optical elements in the path of the beam. After optimizing the prism compressor, the autocorrelation width is reduced to 40 fs, indicating a pulse duration of $t_L = 28$ fs assuming a Gaussian pulse shape.

Figure 3 shows a static photoemission spectrum recorded at $h\nu = 3.15$ eV in $\hat{p}$ polarization with a pulse energy of 150 nJ

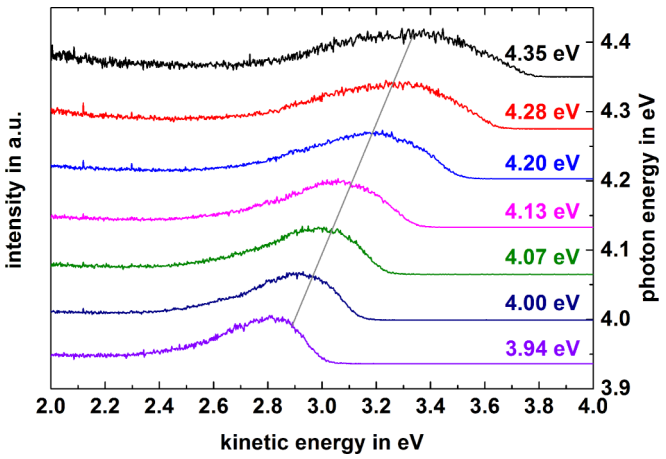

FIG. 2. (Color online) Two-photon photoemission spectra for different photon energies from $h\nu = 3.94$ to 4.35 eV. All spectra are normalized to the linear part of the bulk emission background. The gray line with a slope of $m = (1.04 \pm 0.05)$ indicates the best fit to the position of the higher energy Gaussian peak at E_2.

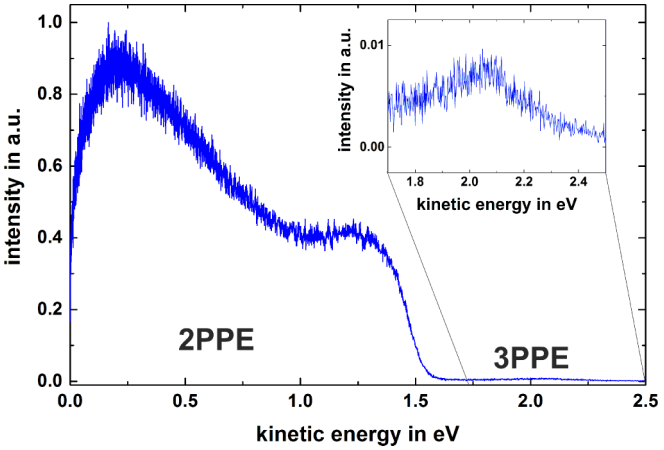

FIG. 3. (Color online) Photoemission spectrum recorded at $h\nu = 3.15$ eV. The main signal is a two-photon emission signal from the bulk gold substrate as indicated in the figure. The inset shows an enlargement of the region in front of the 2PPE Fermi edge, where the three-photon photoemission signal from the unoccupied states of the nanoribbons can be seen.

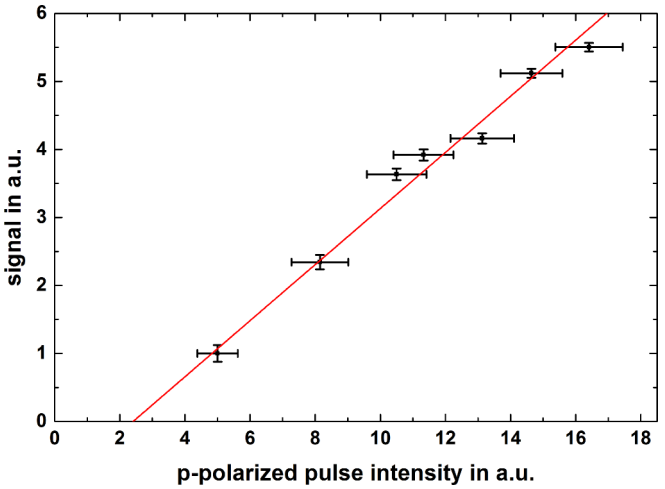

FIG. 4. (Color online) Dependence of the 3PPE signal enhancement for crossed polarizations on the intensity of the $\hat{p}$ polarized pulse with respect to the $\hat{s}$ polarized pulse at time delay $\Delta t = 0$. The line represents a linear fit to the data, indicating a linear dependence of the enhancement on the $\hat{p}$ polarized intensity.

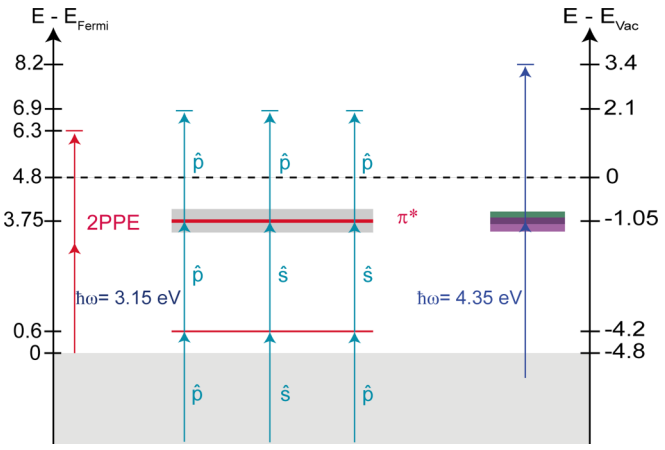

FIG. 5. (Color online) Excitation pathways observed in 3PPE experiments with photon energies of $h\nu = 3.15$ eV and comparison of the accessible binding energies with those found in 2PPE.

and focused to a spot size of 300 μm. Note that the polarization is given with respect to the macroscopic surface normal, which differs from the surface normal of the terraces by 3.52°. The spectrum is dominated by two-photon photoemission from the bulk gold substrate. In front of the Fermi edge another signal can be identified which is magnified in the inset. This signal can be attributed to a 3PPE signal enhanced by the unoccupied states E_1 and E_2. This is also confirmed by a cubic dependence of the integrated signal on the exciting laser pulse energy. When excited with $\hat{s}$ polarized light, no 3PPE signal is detected, indicating a strict selection rule for at least one of the excitation steps.

From the shape of the time resolved measurements (Fig. 6), it is evident that the first excitation is possible in vertical polarization: the slope of the signal is steeper for negative delays, where the $\hat{p}$ polarized precedes the $\hat{s}$ polarized pulse. To determine if the second excitation step is also possible in $\hat{s}$ polarization, the two arms of the interferometer are set to temporal overlap of the two pulses. While keeping the intensity of the $\hat{s}$ polarized arm constant, the intensity of the $\hat{p}$ polarized arm is changed. As shown in Fig. 4, a linear dependence of the 3PPE signal enhancement on the intensity of the $\hat{p}$ polarized laser pulse is observed. We can therefore conclude that the last excitation step is only possible in $\hat{p}$ polarization. Because the GNRs are lying flat on the substrate, σ bonds are in plane and π bonds point in the direction of the surface normal. The polarization dependence then indicates a π^* symmetry for both unoccupied states at E_1 and E_2. In Fig. 5, we show the excitation pathways which are relevant for the 3PPE measurements. The first pathway ($\hat{p}$-$\hat{p}$-$\hat{p}$) is responsible for a constant background in the measurements, while the second pathway ($\hat{s}$-$\hat{s}$-$\hat{p}$) is relevant for the decay found for positive delays and indicates the lifetime of the upper states. Finally, the third pathway ($\hat{p}$-$\hat{s}$-$\hat{p}$) leads to a smeared out slope for negative delay, as the lifetime of the state at $E - E_F = 0.6$ eV enhances the signal for small negative delays where both pulses barely overlap. Note that the pathway($\hat{s}$-$\hat{p}$-$\hat{p}$) is not included in Fig. 5, since at the pulse energies employed for both beams this excitation is suppressed by the much more efficient ($\hat{s}$-$\hat{s}$-$\hat{p}$) pathway, as is also indicated by the linear intensity dependence in Fig 4. To reference the states accessed with 3PPE, the two-photon excitation at $h\nu = 4.35$ eV is added on the right side of the scheme.

To evaluate the time-resolved measurements, we first integrate over the energetic region of interest in the photoemission spectrum for each delay. The corresponding signals are shown in Fig. 6 with positive delays corresponding to the $\hat{s}$ polarized pulse arriving first. The insets show the respective area of integration referenced to the 2PPE signal at $h\nu = 4.35$ eV. At first, a linear background caused by the contribution of the $\hat{p} - \hat{p} - \hat{p}$ excitation pathway is subtracted to isolate the signal enhancement caused by the overlap of the two pulses, which is then fitted using the equation

$$I(\delta t) = \left[\left(A_{\hat{s}}^2 * A_{\hat{p}}\right)(t)\right] * \left[\theta(\delta t - t)\exp\left(-\frac{\delta t}{\tau}\right)\right].$$

Here, $A_{\hat{s}}$ and $A_{\hat{p}}$ are the intensities of the laser pulse in the respective polarization, the $*$ denotes the convolution operator, θ is the Heaviside step function, and τ is the fit parameter and corresponds to the lifetime of the unoccupied state. The first convolution $(A_{\hat{s}}^2 * A_{\hat{p}})(t)$ accounts for the fact that two photons from the $\hat{s}$ polarized pulse and only one photon from the $\hat{p}$ polarized pulse contribute to the signal enhancement near the overlap of the pulses. Both $A_{\hat{s}}$ and $A_{\hat{p}}$ are represented by a Gaussian pulse with a duration of 28 fs (FWHM) as found in the autocorrelation measurements. After this, the resulting pulse is convoluted with an exponential decay to describe the lifetime of the unoccupied state.

When integrating over the part of the 3PPE signal that is dominated by the first unoccupied state ($E_1 - E_F =$ [3.1,3.6] eV), we derive a lifetime of $\tau_1 = (110 \pm 13)$ fs independent of $\vec{k}_{||}$ along the long axis of the nanoribbons. Employing the same evaluation method to the 3PPE signal from the second unoccupied state ($E_2 - E_F =$ [3.7,4.2] eV), an electronic lifetime of $\tau_2 = (75 \pm 10)$ fs is derived, which is also independent of $\vec{k}_{||}$ within our experimental resolution.

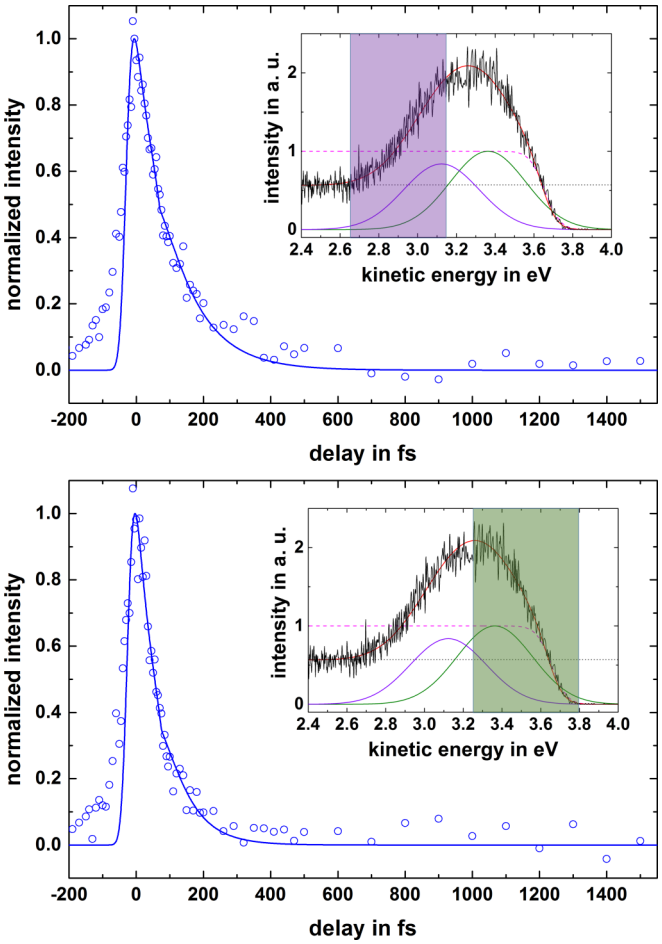

FIG. 6. (Color online) Time-resolved three-photon photoemission measurement (circles) and fit to the measurement (line). The shaded area in the inset shows the energy area of integration with respect to the states found in 2PPE with $h\nu = 4.35$ eV. (a) When integrating over the region dominated by the lower excited state ($E_1 - E_F = [3.1,3.6]$ eV) a lifetime of $\tau_1 = (110 \pm 13)$ fs is derived. (b) Integrating over the region dominated by the upper excited state ($E - E_F = [3.7,4.2]$ eV). Here a lifetime of $\tau_2 = (75 \pm 10)$ fs is found.

These lifetimes are considerably longer than those found for a graphene layer on noble metals in the same energetic region. In that case, lifetimes of around 23 and 30 fs were measured for Au-intercalated Ni(111) and Au-intercalated Ir(111) substrates, respectively [15]. The difference can be explained by the different nature of the involved states. The states investigated by Nobis *et al.* were identified as image potential states (IPS), which are known to have a wave function that decays inside the bulk and is nonzero for several atomic layers. The decay mechanism of IPS is not strongly related to the electronic coupling between substrate and graphene because of the nature of the wave functions of these excited states [15]. Consequently, we expect an efficient decay mechanism for the IPS regardless of the interaction between metal and graphene. The non-IP states of GNR instead relax more slowly, because of the low DOS around E_F and the weak interaction that is expected for graphene nanoribbons on gold.

Some insight into the decay mechanism in 7a-GNRs can be gained by comparing these lifetimes to those found in single-wall carbon nanotubes (SWCNTs), which also represent a graphene-like, quasi-one-dimensional material with unoccupied molecular orbitals rather than image states. In bucky paper consisting mainly of SWCNTs with a diameter of 12 Å, the decay times of the second and third unoccupied state are quite similar to those observed for 7-aGNRs, amounting to $\tau_2 = 130$ fs and $\tau_3 = 72$ fs, respectively [16].

III. CONCLUSION

In conclusion, we measured the electronic lifetimes of two different unoccupied states in aligned 7-aGNRs on Au(788) located at $E_1 - E_F = 3.6$ eV and $E_2 - E_F = 3.8$ eV, respectively, by time-resolved 3PPE. The excitation of these states was facilitated by a resonance between an intermediate midgap state at $E_i - E_F = 0.7$ eV, confirming the results of previous IPE measurements. The measured lifetimes of $\tau_1 = (110 \pm 13)$ fs and $\tau_2 = (75 \pm 10)$ fs are much shorter than those measured for image pontential states of sheet graphene on different metal substrates due to more efficient decay channels. They are, however, in good agreement with the lifetimes of the respective unoccupied states of SWCNTs.

ACKNOWLEDGMENTS

This work was supported by the Deutsche Forschungsgemeinschaft (DFG) through Priority Program SPP 1459 and the Transregional Collaborative Research Center TRR 61 (Project B9).

[1] K. S. Novoselov, A. K. Geim, S. V. Morozov, D. Jiang, Y. Zhang, S. V. Dubonos, I. V. Grigorieva, and A. A. Firsov, Science **306**, 666 (2004).
[2] F. Schwierz, Nat. Nanotechnol. **5**, 487 (2010).
[3] Y.-M. Lin, C. Dimitrakopoulos, K. A. Jenkins, D. B. Farmer, H.-Y. Chiu, A. Grill, and P. Avouris, Science **327**, 662 (2010).
[4] Z. Chen, Y.-M. Lin, M. J. Rooks, and P. Avouris, Physica E **40**, 228 (2007).
[5] L. Jiao, L. Zhang, X. Wang, G. Diankov, and H. Dai, Nature (London) **458**, 877 (2009).
[6] D. V. Kosynkin, A. L. Higginbotham, A. Sinitskii, J. R. Lomeda, A. Dimiev, B. K. Price, and J. M. Tour, Nature (London) **458**, 872 (2009).
[7] M. Y. Han, J. C. Brant, and P. Kim, Phys. Rev. Lett. **104**, 056801 (2010).
[8] J. Cai, P. Ruffieux, R. Jaafar, M. Bieri, T. Braun, S. Blankenburg, M. Muoth, A. P. Seitsonen, M. Saleh, X. Feng, K. Müllen, and R. Fasel, Nature (London) **466**, 470 (2010).
[9] L. Yang, C.-H. Park, Y.-W. Son, M. L. Cohen, and S. G. Louie, Phys. Rev. Lett. **99**, 186801 (2007).

[10] Y. H. Lu, R. Q. Wu, L. Shen, M. Yang, Z. D. Sha, Y. Q. Cai, P. M. He, and Y. P. Feng, Appl. Phys. Lett. **94**, 122111 (2009).
[11] P. B. Bennett, Z. Pedramrazi, A. Madani, Y.-C. Chen, D. G. de Oteyza, C. Chen, F. R. Fischer, M. F. Crommie, and J. Bokor, Appl. Phys. Lett. **103**, 253114 (2013).
[12] S. Linden, D. Zhong, A. Timmer, N. Aghdassi, J. H. Franke, H. Zhang, X. Feng, K. Müllen, H. Fuchs, L. Chi, and H. Zacharias, Phys. Rev. Lett. **108**, 216801 (2012).
[13] C. Bronner, F. Leyssner, S. Stremlau, M. Utecht, P. Saalfrank, T. Klamroth, and P. Tegeder, Phys. Rev. B **86**, 085444 (2012).
[14] P. Ruffieux, J. Cai, N. C. Plumb, L. Patthey, D. Prezzi, A. Ferretti, E. Molinari, X. Feng, K. Müllen, C. A. Pignedoli, and R. Fasel, ACS Nano **6**, 6930 (2012).
[15] D. Nobis, M. Potenz, D. Niesner, and T. Fauster, Phys. Rev. B **88**, 195435 (2013).
[16] T. Hertel and G. Moos, Chem. Phys. Lett. **320**, 359 (2000).